TRENDS IN SCIENCES 2026; 23(11): 13966
https://doi.org/10.48048/tis.2026.13966 RESEARCH ARTICLE

Structure–Function Correlation in ZnO-Modified PVDF-HFP Nanofibers Enabling Antibacterial Membrane Performance

Paweena Porrawatkul[1], Sirikun Pethuan[1], Jureeporn Yuennan[1,*], Nikruesong Tohluebaji[2], Ponkanok Dawan[3], Pitsinee Supakitanan[3], Arachaporn Vijara[3], Ratchaneewan Siri[4], Nantakan Muensit[4], Chatchai Putson[4], Thammarong Eadkhong[5] and Phongpichit Channuie[5]

[1]Faculty of Science and Technology, Nakhon Si Thammarat Rajabhat University, Nakhon Si Thammarat 80280, Thailand
[2]Faculty of Science and Technology, Princess of Naradhiwas University, Narathiwat 96000, Thailand
[3]Benjamarachutit School, Nakhon Si Thammarat 80280, Thailand
[4]Division of Physical Science (Physics), Faculty of Science, Prince of Songkla University, Songkhla 90112, Thailand
[5]School of Science, Walailak University, Nakhon Si Thammarat 80160, Thailand

([*]Corresponding author's e-mail: jureeporn_yue@nstru.ac.th)

Received: March 31, 2026, Revised: May 26, 2026, Accepted: 5 June 2026, Published: 30 June 2026

Abstract

Electrospun nanofibers of poly(vinylidene fluoride-co-hexafluoropropylene) (PVDF-HFP) were successfully functionalized with zinc oxide (ZnO) nanoparticles (NPs) to develop multifunctional membranes with enhanced hydrophobicity and antibacterial performance, aimed at self-cleaning air filtration applications. ZnO NPs, synthesized via a precipitation method and deposited at various loadings (5 - 20 wt%), were uniformly coated on the surfaces of PVDF-HFP nanofibers, as confirmed by SEM-EDX, FTIR, and XRD analyses. The incorporation of ZnO significantly increased the crystallinity of the nanofibers from 25.1% for uncoated fibers to 55.4% at 20 wt% ZnO content, improving both structural ordering and thermal resistance up to 525 °C. Notably, the 5 wt% ZnO-coated composite exhibited the highest water contact angle of 143.5° and the lowest surface energy of 7.4 mJ/m², indicating superior hydrophobicity favorable for self-cleaning. Furthermore, mechanical testing revealed balanced tensile strength of 2.48 MPa and flexibility at moderate ZnO loadings (10% - 15%), demonstrating strong interfacial bonding between ZnO NPs and the polymer matrix. Antibacterial assays against *Staphylococcus aureus* and *Staphylococcus epidermidis* showed clear inhibition zones up to 17.1 mm, confirming potent bactericidal efficacy arising from reactive oxygen species generation and Zn^{2+} ion release. Collectively, these results highlight that ZnO/PVDF-HFP nanofiber membranes possess high hydrophobicity, thermal stability, mechanical durability, and antibacterial activity, making them promising candidates for smart air filtration and protective mask applications.

Keywords: PVDF-HFP, ZnO, Electrospinning, Hydrophobicity, Antibacterial activity

Introduction

Bacteria and other microorganisms are widely present in both indoor and outdoor air, existing either as aerosols or attached to dust particles. Their source includes human activities, such as coughing and sneezing, as well as emissions from animals, plants, and environmental sources like soil and surface debris. Airborne bacteria exhibit considerable size variations; for example, *Staphylococcus aureus* (*S. aureus*) typically measures approximately 0.5 - 1 μm, *Bacillus subtilis* ranges from 1 - 2 μm, *Pseudomonas spp.* is commonly found in ventilation systems, and *Escherichia coli* is frequently present in dust. These microorganisms often form particle-laden aerosols with diameters 1 - 10 μm. This size range is particularly important for filter design, as pores smaller than the particle size can effectively capture them. The COVID-19 pandemic has further highlighted the inherent limitations of conventional protective equipment against airborne pathogens [1]. Airborne viruses generally exhibit diameters in the range of 50 - 200 nm [2], making them difficult to block completely with standard face masks. Given the low infectious dose of a few hundred virions [3], masks must achieve exceptionally high filtration efficiency, particularly to healthcare workers subjected to extended and repeated exposure [4,5]. While standard surgical masks are typically designed to filter particles with sizes down to approximately 0.3 μm, nanofiber-based filters offer a markedly higher fiber packing density and specific surface area, enabling more effective capture of both nanoscale and larger airborne particulates. In addition, airborne bacterial concentrations typically range from 10^3 - 10^4 CFU/m^3 in general indoor environments, with substantially elevated levels in hospital settings, food industries, and densely populated areas. Individuals with compromised immune systems are at greater risk of respiratory infections, which may lead to chronic conditions, escalate medical expenses, increase reliance on antibiotics, prolong recovery periods, and reduced overall productivity. Recurrent infections further increase the risk of pathogen transmission, facilitating outbreaks within communities and healthcare facilities. Therefore, preventing airborne bacterial infections remains a critical public health challenge. Conventional face masks and filtration systems often exhibit limited efficiency in capturing nanoparticles (NPs) and inhibiting microbial growth, underscoring the urgent need for advanced technologies. In this context, antibacterial nanofiber-based air filters have emerged as promising strategies to more effectively mitigate pathogen spread and reduce their impact.

Poly(vinylidene fluoride-co-hexafluoropropylene) (PVDF-HFP) is a fluorinated copolymer that combines the advantageous properties of poly(vinylidene fluoride (PVDF) and hexafluoropropylene (HFP), resulting in several important physical and chemical characteristics [6,7]. The copolymer shows excellent solubility in polar aprotic solvents, including dimethylformamide (DMF)/acetone [8], N,N-dimethylacetamide, N-methyl-2-pyrrolidone [9], and dimethyl sulfoxide [10], which enables the production of nanofibers via electrospinning [11,12]. PVDF-HFP can crystallize into four distinct phases: α, β, γ, and δ, among which the α-phase predominates. However, exposure to a sufficiently strong electric field during electrospinning promotes the transformation of the α-phase to the β-phase [13]. Owing to its superior mechanical strength, chemical stability, and thermal resistance, PVDF-HFP is applied in diverse industrial contexts, including polymeric electrolyte membranes for fuel cells, chemical sensors, desalination systems, separation membranes, and primarily as filtration materials. Several PVDF membranes are commonly fabricated using inorganic nanomaterials and/or other organic polymers [14]. The polymer exhibits notable mechanical flexibility and thermal stability, withstanding temperatures up to 140 - 160 °C, and demonstrates strong resistance to acidic, basic, and organic solvent environments, making it suitable for operation under harsh chemical conditions. PVDF-HFP further possesses piezoelectric [15] and dielectric [14] properties, enabling applications in sensing and actuation technologies. The surface characteristics of PVDF-HFP can be tailored by adjusting electrospinning parameters, such as humidity, solvent viscosity, and tip-to-collector distance. Moreover, the intrinsic hydrophobicity and antimicrobial performance can be significantly enhanced by incorporating NPs, such as zinc oxide (ZnO) [9], silver-ZnO [16], or titanium dioxide [17], leading to improved bacterial resistance and filtration efficiency. Electrospun PVDF-HFP nanofiber membranes possess a high surface area-to-volume ratio,

allowing effective capture of dust particles and nanoscale contaminants. Its inherent hydrophobicity also enhances the filtration of water droplets and bioaerosols, thereby making PVDF-HFP an excellent material for the development of advanced antibacterial air filtration membranes.

ZnO NPs are metal oxide nanomaterials that have attracted significant attention due to their unique physicochemical and functional properties [18]. ZnO is an II-VI semiconductor with a direct wide band gap of approximately 3.3 eV and a relatively high excitonic binding energy of ~60 meV [19]. As a result, ZnO demonstrates excellent optical [20] and electrical [21] characteristics, along with high chemical stability, photostability, and thermal resistance. Moreover, its large specific surface area, light weight and excellent mechanical properties [22] further support its suitability for a wide range of applications, including catalysis [23], photoelectronic devices, cosmetics, and antimicrobial agents [24]. At the nanoscale, ZnO demonstrates an enhanced surface area-to-volume ratio, leading to greater surface reactivity and biological activity [25]. The antibacterial mechanism of ZnO-NPs is primarily attributed to the generation of reactive oxygen species (ROS) and the release of Zn^{2+} ions, particularly under UV illumination. These processes induce oxidative stress and disrupt bacterial cell membranes, ultimately leading to cell death [26]. Interestingly, Rohani *et al.* [27] reviewed the green synthesis of ZnO NPs, emphasizing eco-friendly biological methods capable of producing NPs with excellent antimicrobial and photocatalytic properties, alongside broad applications in medicine, environmental protection, and agriculture. Similarly, Yagoub *et al.* [28] reported that ZnO NPs synthesized using *Lavandula pubescens* methanolic extract displayed strong antibacterial and antifungal activities against *Pseudomonas aeruginosa*, *Staphylococcus aureus*, *Aspergillus niger*, and *Aspergillus terreus*, with a notable enhancement in efficacy ascribed to the synergistic effect of the plant extract.

In this study, ZnO NPs were incorporated onto electrospun PVDF-HFP nanofibrous membranes to develop multifunctional materials exhibiting both hydrophobic and antibacterial functionalities for self-cleaning air filtration applications. The surface modification with ZnO was expected to enhance the crystallinity, thermal stability, and mechanical durability of the polymer matrix, while simultaneously imparting strong antibacterial activity through ROS generation and controlled Zn^{2+} ion release. Careful optimization of ZnO incorporation was intended to yield nanocomposite membranes with superior water repellency, tunable surface energy, and efficient inhibition of bacterial growth. The systematic characterization of the ZnO/PVDF-HFP nanofiber membranes in terms of morphology, structural, thermal, mechanical, hydrophobic, and antibacterial characteristics provides valuable insight into their potential as advanced smart-filter materials for respiratory protection and environmental purification.

Materials and methods

Materials

PVDF-HFP, Solef® 11010/1001, was utilized as the base polymer for nanofiber fabrication. The polymer, supplied by Solvay (Bangkok, Thailand), possessed a density of 1.78 g/cm³ and a melting temperature range of 158 - 162 °C. Polymer solutions were prepared by dissolving 25 g of PVDF-HFP in 100 mL of DMF (AR1051-G4L, density 0.949 g/cm³), a polar solvent obtained from RCI Labscan (Thailand). ZnO NPs were synthesized using zinc acetate dihydrate ($Zn(CH_3COO)_2 \cdot 2H_2O$) and sodium hydroxide (NaOH), both of which were purchased from Sigma-Aldrich.

Method for fabrication of nanofibers

The PVDF-HFP mixture was stirred thoroughly until a homogeneous solution was achieved. Electrospinning was conducted using a horizontal setup consisting of a high-voltage power supply (Trek model 610E, USA), a syringe pump (Nz1000, NEWERA Pump Systems Inc., USA), and a grounded rotating collector covered with aluminum foil, as represented in **Figure 1(a)**. The prepared solution was loaded into a 20 mL syringe fitted with a stainless-steel needle (20.5 gauge). The solution was delivered at a controlled flow rate of 0.5 mL/h, while an applied voltage of 15 kV was applied across a fixed tip-to-collector distance of 10 cm. Electrospinning was carried out at room temperature, with a relative humidity of 50% - 60%. Collected nanofibers were dried in a hot-air oven at 60 °C for 12 h to ensure complete removal of residual solvents.

As illustrated in **Figure 1(b)**, PVDF-HFP nanofiber mats were functionalized by coating them with ZnO NPs. The ZnO coating solutions were prepared by dissolving synthesized ZnO powder in alcohol at concentrations of 5%, 10%, 15%, and 20%, followed by continuous stirring for 20 min. The sheets were then cut into pieces of approximately 3×3 cm and immersed in the respective ZnO solutions. To ensure uniform nanoparticle dispersion and effective infiltration, the immersed samples underwent ultrasonic treatment in a water bath for 30 min. After sonication, the sheets were gently pressed with a metal ruler to promote deeper ZnO penetration into the fiber matrix. The treated samples were subsequently placed in clean Petri dishes and dried in a hot-air oven at 60 °C for 2 h. Finally, the dried sheets were punched into circular discs and used for subsequent bacterial culture testing.

Characterization method

As shown in **Figure 1(d)**, the morphology of the electrospun nanofibers was examined using scanning electron microscopy (SEM; Hitachi SU3900, Hitachi, Japan) operated at an accelerating voltage of 10 kV. The ZnO and PVDF-HFP powders, along with the electrospun PVDF-HFP/ZnO nanofiber composites, were analyzed to evaluate surface morphological features and structural uniformity. Quantitative analysis of particle size and fiber diameter was performed using ImageJ software (National Institutes of Health, USA) based on SEM micrographs, enabling a detailed assessment of size distribution and fiber consistency. Elemental composition was further analyzed using energy-dispersive X-ray spectroscopy (EDX; Quanta 400).

The surface wettability of the prepared fiber mats was evaluated through water contact angle (WCA) measurements using a Data Physics Contact Angle System (OCA-15EC, Germany) operating in sessile drop mode. For each measurement, a 2 µL droplet of distilled water was carefully deposited onto 1×1 cm fiber mats, and the mean contact angle was calculated from at least three replicates per sample. The chemical structure of the nanofibers was examined by Fourier-transform infrared spectroscopy (FTIR; Bruker Vertex 70, Germany) operated in attenuated total reflection mode, with spectra recorded across the wavenumber range of 4,000 - 400 cm^{-1}. The crystalline phases and crystallite sizes were determined by X-ray diffraction (XRD; Empyrean, PANalytical, Netherlands) utilizing Cu-Kα radiation (λ = 0.154 nm) at an accelerating voltage of 40 kV and a current of 30 mA. Diffraction patterns were acquired within a 2θ range of 5° - 90°, with a step size of 0.026° and a dwell time of 70.125 s per step. The degree of crystallinity (*%Xc*) of the nanofibers was calculated using the equation: $\%Xc = (A_{total}/A_{peak}) \times 100$. Thermal stability was assessed through thermogravimetric analysis (TGA; TGA 8000, PerkinElmer, USA) under a nitrogen atmosphere at a flow rate of 20 mL/min, with the temperature increased from 50.00 - 700.00 °C at a heating rate of 10.00 °C/min. Mechanical properties, including tensile strength and elongation at break (%), were measured using a universal testing machine (Z010, ZwickRoell, Germany) under uniaxial loading conditions.

In addition, ZnO NPs were systematically characterized to support the composite analysis. Morphological features were investigated using transmission electron microscopy (TEM; Thermo Scientific™ Talos™ F200i, Czech Republic) operated at 200 kV, providing high-resolution images of structure and dispersion. The surface morphology of the ZnO microspheres was further analyzed using SEM. To obtain comprehensive physicochemical insights, TGA, XRD, and FTIR were employed to evaluate thermal stability, crystalline structure, and chemical composition of the ZnO NPs.

Bacterial culture and antibacterial testing of ZnO-coated nanofiber sheets

As illustrated in **Figure 1(c)**, the antibacterial activity of ZnO-coated PVDF-HFP nanofiber sheets was evaluated using the disk diffusion assay against Staphylococcus epidermidis (S. epidermidis) and Staphylococcus aureus (S. aureus) as representative Gram-positive bacteria. The bacterial strains were obtained from the National Institute of Health of Thailand, Department of Medical Sciences, Ministry of Public Health. Initially, both strains were streaked onto nutrient agar plates and incubated at 37 °C to obtain isolated colonies. A sterile inoculating loop was then used to transfer the colonies into nutrient broth tubes, followed by incubation at 37 °C for 24 h to promote bacterial growth. The cultured bacterial suspensions were diluted with sterile saline solution, and the

turbidity was adjusted to 0.5 McFarland standard (approximately 1.5×10^8 CFU/mL). A sterile cotton swab was immersed in the adjusted bacterial suspension and evenly spread onto fresh nutrient agar plates. ZnO-coated PVDF-HFP nanofiber sheets with a diameter of 0.5 cm containing 5%, 10%, 15%, and 20% ZnO were gently placed onto the inoculated agar surfaces, while uncoated PVDF-HFP nanofiber sheets were used as the control samples. The plates were incubated at 37 °C for 24 h, after which the diameters of the inhibition zones surrounding each sample were measured using a digital caliper. All antibacterial measurements were performed in triplicate, and the average inhibition zone diameters were calculated to compare antibacterial efficacy among different ZnO loadings and bacterial strains.

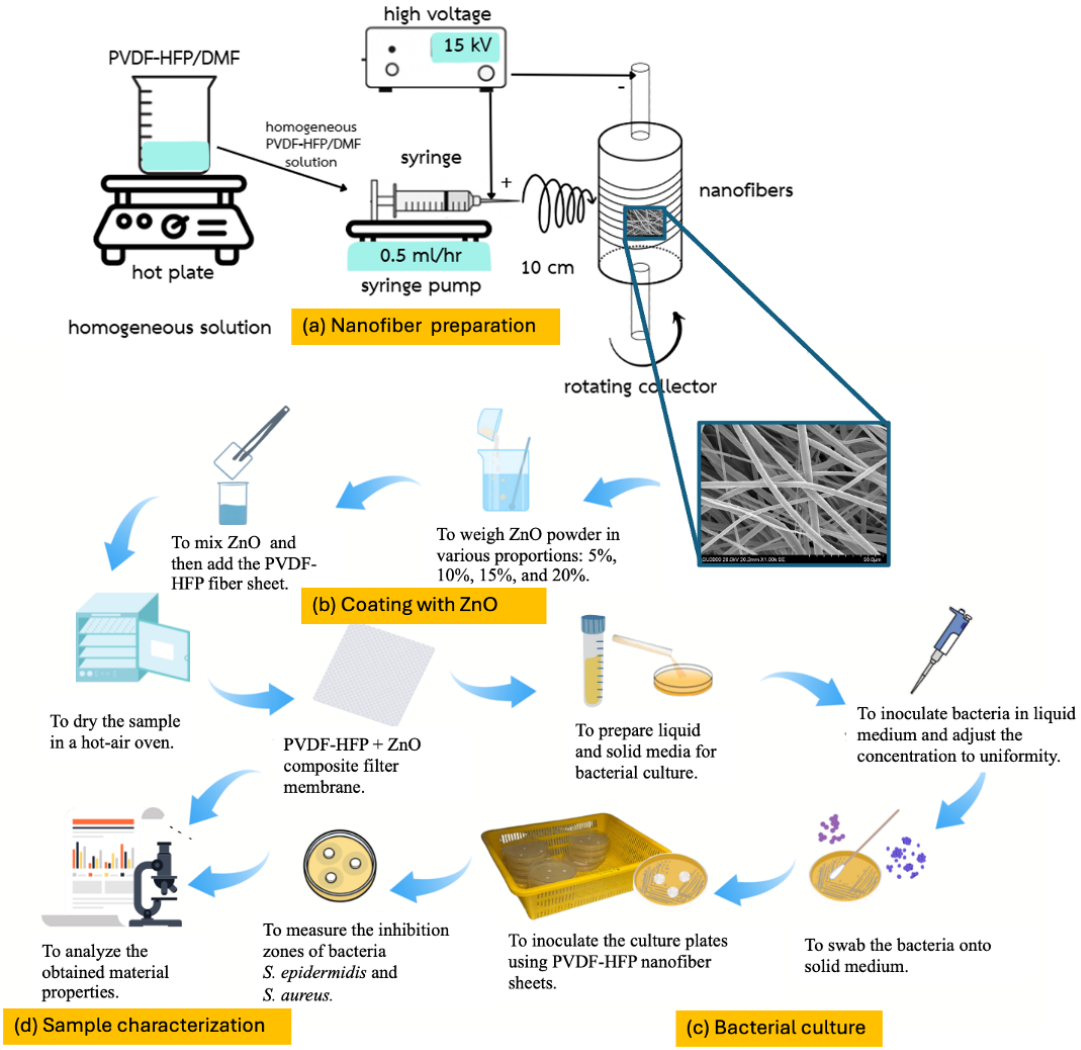

Figure 1 Schematic diagram of the experimental process for PVDF-HFP/ZnO composite nanofibers: (a) Nanofiber preparation by electrospinning PVDF-HFP solution, (b) coating with ZnO at 5 wt% - 20 wt% and drying to form composite membranes, (c) bacterial culture of *S. epidermidis* and *S. aureus* for antibacterial testing, and (d) sample characterization by inhibition zone measurement and material analysis.

Results and discussion

TEM analysis

The morphology and structure of materials were studied by transmission electron microscopy (TEM), which is well established and widely used to characterize materials. successful synthesis and structural integrity of the ZnO nanostructures. TEM micrographs (**Figure 2(a)**) showed a plate-like morphological structure of ZnO NPs, which can be attributed to the anisotropic crystal growth behavior of hexagonal wurtzite ZnO during the precipitation process. The preferential lateral growth along specific

crystallographic planes promoted the formation of platelet-like nanostructures [29]. These observations, consistent with the results obtained from XRD, FT-IR, and EDX-SEM analyses, confirmed the.

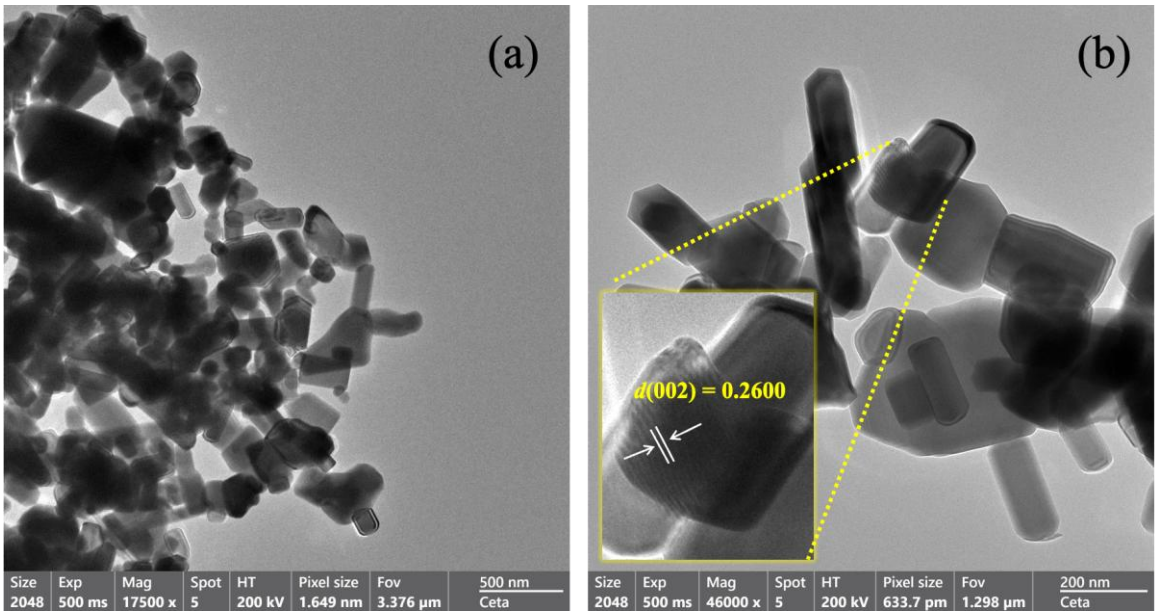

Figure 2 TEM micrograph of the commercial ZnO nanoparticles (a) at a magnification of 17.5 kx and (b) at magnification of 46 kx.

SEM and EDX analysis

SEM was appointed to observe the surface morphology, particle size, and distribution of ZnO and PVDF-HFP powders. As shown in **Figure 3(a)**, ZnO exhibits a plate-like, morphology with a relatively rough surface, typical of NPs synthesized via the precipitation process. The corresponding particle size distribution displayed in **Figure 3(c)** shows a mean diameter of 0.15 µm with a standard deviation of ±0.0037 µm, indicating a uniform nanoscale size. Uniform nanoscale particle distribution provides a larger accessible surface area and promotes more homogeneous interfacial contact between ZnO nanoparticles and PVDF-HFP chains. The increased surface-to-volume ratio exposes a greater number of active surface sites, thereby enhancing interfacial interactions between the ZnO surface hydroxyl groups and the fluorinated functional groups of PVDF-HFP. In addition, homogeneous nanoparticle dispersion minimizes local aggregation and facilitates more efficient stress transfer within the composite structure. These findings are consistent with the results reported by Mohammed *et al.* [30], who observed that ZnO NPs of comparable dimensions exhibit enhanced surface activity and strong interfacial adhesion in polymer-based nanocomposites. In contrast, the PVDF-HFP powder displays a smooth, dense, and spherical morphology (**Figure 3(b)**), which is characteristic of semicrystalline fluoropolymers. This morphology is mainly attributed to the strong intermolecular interactions and compact chain packing within the semicrystalline PVDF-HFP structure, resulting in reduced surface irregularities and the formation of dense polymer granules during powder processing. The spherical morphology also contributes to improved flowability and homogeneous dispersion during solution preparation and electrospinning. The particle size distribution (**Figure 3(d)**) shows a mean diameter of 135 µm with a narrow standard deviation of ±0.66 µm, confirming the high uniformity of the polymer granules. The particle size distribution (**Figure 3(d)**) shows a mean diameter of 135 µm with a narrow standard deviation of ±0.66 µm, confirming the high uniformity of the polymer granules. Such morphological regularity facilitates homogeneous dispersion during electrospinning, ensuring stable fiber formation and efficient coating of ZnO NPs.

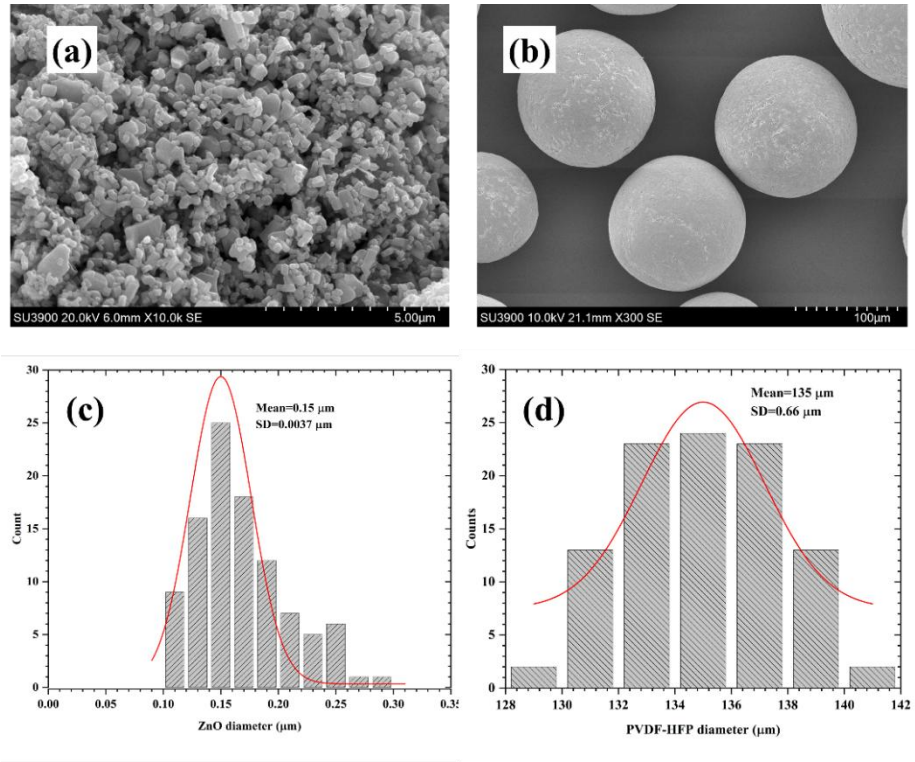

Figure 3 SEM images and particle size distributions of ZnO and PVDF-HFP powders: (a) ZnO, (b) PVDF-HFP, (c) ZnO particle size distribution, and (d) PVDF-HFP particle size distribution.

PVDF-HFP powder was transformed into nanofiber sheets using the electrospinning method. The surface morphology of both uncoated and ZnO-coated nanofiber sheets was examined using SEM. As shown in **Figure 4(a)**, the uncoated PVDF-HFP nanofibers exhibit a smooth, homogeneous, and bead-free surface, suggesting well-controlled and stable electrospinning conditions. The corresponding fiber diameter distribution (**Figure 4(b)**) indicates randomly oriented fibers with high porosity and an average diameter of 2.75 ± 0.06 μm. The random orientation originates from the chaotic bending instability and whipping behavior of the charged polymer jet during electrospinning under a strong electric field, resulting in non-uniform fiber deposition on the collector surface. In addition, rapid solvent evaporation combined with continuous fiber deposition and overlapping accumulation generates interconnected pores and a highly porous three-dimensional fibrous network. Such morphology is characteristic of electrospun membranes and contributes to enhanced specific surface area and improved functional properties. Following coating with ZnO NPs, noticeable morphological variations are evident (**Figures 4(c) - 4(f)**). At 5 wt% ZnO loading, the NPs are sparsely yet homogeneously attached to the fiber surface. When the ZnO content increases to 10% and 15%, the NPs form a denser and more continuous surface layer, suggesting improved interfacial adhesion between the ZnO NPs and the polymer matrix, albeit with slight aggregation. Conversely, at 20 wt% ZnO loading, excessive particle deposition causes distinct agglomeration, partially obscuring the fibrous structure and increasing surface roughness. These morphological changes confirm the successful attachment of ZnO NPs on the PVDF-HFP nanofiber surfaces, with coating density rising proportionally to ZnO concentration. The enhanced surface roughness at higher ZnO levels is anticipated to increase the specific surface area and, consequently, improve antibacterial efficiency by increasing the exposed ZnO active sites. However, severe nanoparticle aggregation at higher ZnO loadings may adversely affect fiber uniformity and mechanical performance, as previously reported by Pethuan *et al.* [31] and Șomoghi *et al.* [32]. Excessive agglomeration introduces localized stress concentration regions and disrupts the homogeneous distribution of nanoparticles within the fibrous structure, resulting in structural heterogeneity and increased defect formation.

Furthermore, large ZnO aggregates reduce the effective interfacial contact area between the nanoparticles and the PVDF-HFP matrix, thereby limiting stress transfer efficiency and weakening interfacial adhesion. Consequently, the tensile strength, elongation at break, and overall mechanical integrity of the composite nanofibers may deteriorate at excessive ZnO concentrations.

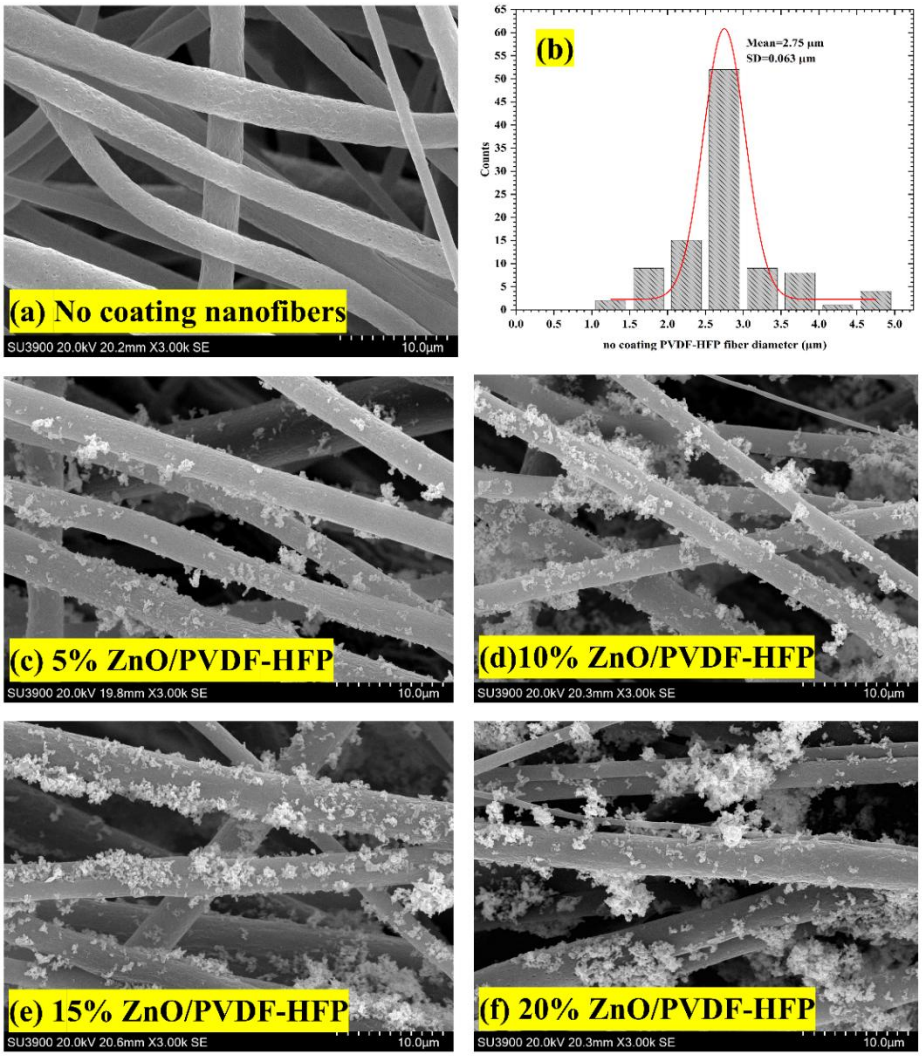

Figure 4 SEM micrographs of (a) uncoated PVDF-HFP nanofibers, (b) fiber diameter distribution, and (c - f) ZnO/PVDF-HFP composite nanofibers coated with 5%, 10%, 15%, and 20% ZnO, respectively.

Furthermore, the elemental composition and distribution of pure PVDF-HFP and ZnO/PVDF-HFP composite nanofibers were analyzed using EDX. As shown in **Figure 5(a)**, the spectrum of the uncoated PVDF-HFP nanofibers exhibits prominent signals of F (57.5 wt%), C (41.5 wt%), and O (1.0 wt%), which is consistent with the chemical structure of the fluoropolymer and indicates the high purity of the electrospun fibers. After coating with the ZnO NPs, the EDX spectrum reveals the emergence of distinct Zn and O peaks, confirming the successful deposition of ZnO on the fiber surfaces (**Figures 5(b) - 5(e)**). The Zn peak originates from zinc atoms, while the O peak corresponds to oxygen atoms in the ZnO crystal lattice. Compared with pristine PVDF-HFP nanofibers, which mainly exhibit C and F signals, the appearance of Zn and O peaks clearly confirms the incorporation of ZnO nanoparticles into the composite nanofibers. Furthermore, the absence of impurity-related elemental peaks indicates the high purity of the synthesized ZnO and the structural homogeneity of the composite system. With increasing ZnO concentration from 5% to 20%, a progressive reduction in the relative intensities of F and C is noted, accompanied by a corresponding increase in

the Zn and O signals, reflecting the gradual enrichment of ZnO within the composite nanofibers. In addition, the EDX elemental mapping demonstrates the uniform distribution of F, C, O, and Zn over the nanofiber surfaces. At lower ZnO concentrations (5% - 10%), the NPs remain evenly dispersed, whereas higher concentrations (15% - 20%) lead to the formation of localized Zn aggregates, which is in agreement with the morphological features observed by SEM. Moreover, the absence of unexpected elemental signals in the EDX spectra confirms the high compositional purity and structural homogeneity of the as-prepared ZnO/PVDF-HFP nanofiber composites.

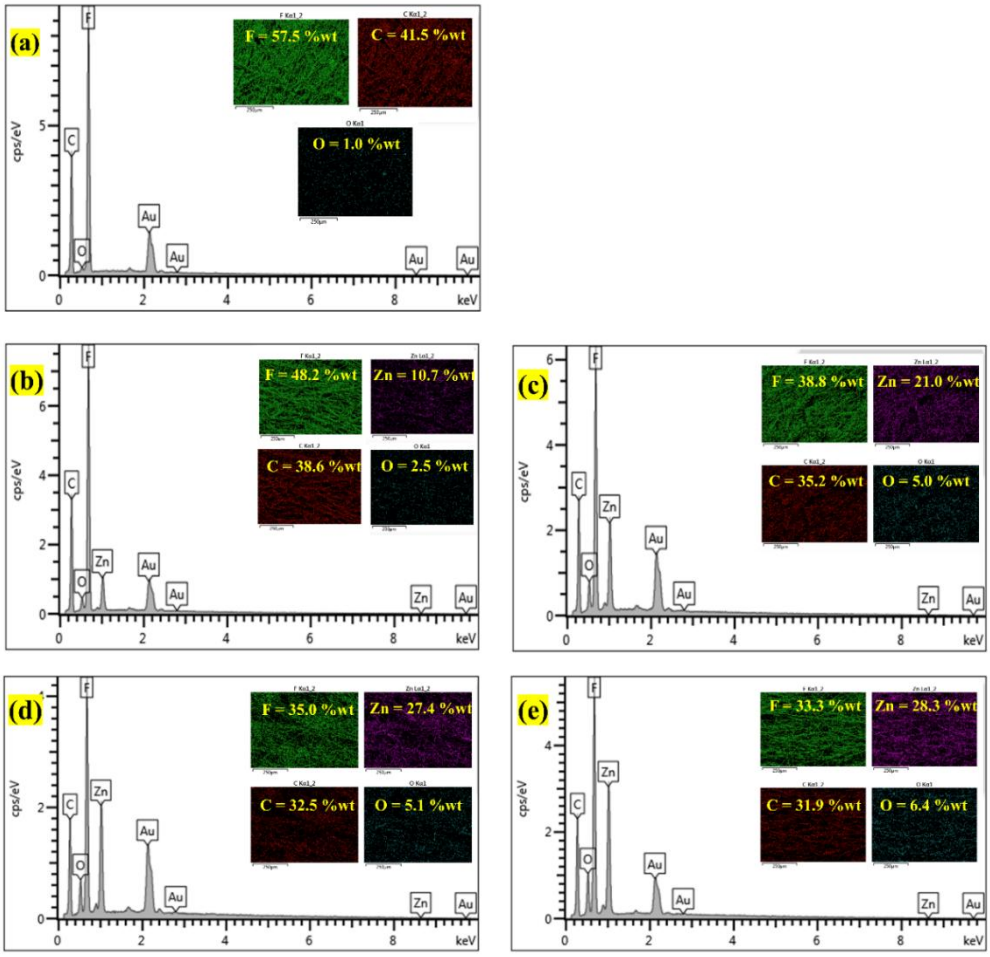

Figure 5 EDX and mapping of (a) uncoated PVDF-HFP fiber (b - e) ZnO/PVDF-HFP composite nanofibers coated with (b) 5%, (c) 10%, (d) 15%, and (e) 20% ZnO.

Hydrophobicity

Variations in WCA and surface energy as a function of ZnO concentrations demonstrate the influence of NP loading on the surface morphology and wettability of PVDF-HFP nanofiber membranes (**Figure 6**). The pristine PVDF-HFP nanofibers display a WCA of 140.6° ± 0.8° and a surface energy of 9.2 ± 0.3 mJ/m^2, confirming their intrinsic hydrophobic character arising from the presence of fluorinated –CF_2– and –CF_3– groups [33]. Upon the incorporation of 5 wt% ZnO, the WCA increases to 143.5° ± 1.7°, while the surface energy decreases to 7.4 ± 0.4 mJ/m^2, indicating improved hydrophobicity. This enhancement can be attributed to the uniform dispersion of ZnO NPs, which introduces micro/nanoscale surface roughness. Such structural features promote air trapping beneath water droplets, in line with the Cassie-Baxter model [34]. The combined effect of increased surface roughness and nonpolar surface chemistry effectively minimizes solid-liquid interfacial interactions. The rough surface morphology can trap air pockets beneath water droplets, thereby reducing the effective contact area between the

liquid and solid surface in accordance with the Cassie-Baxter wetting mechanism. In addition, the fluorinated nonpolar functional groups of PVDF-HFP possess intrinsically low surface energy, which weakens intermolecular interactions with polar water molecules. Consequently, water spreading is suppressed, leading to enhanced hydrophobicity and increased water contact angle values.

As the ZnO concentration increases to 10% - 20%, a gradual reduction in WCA is observed, accompanied by a marked rise in surface energy from 5.1 mJ/m^2 at 10 wt% to 16.3 mJ/m^2 at 20 wt%. This decrease in WCA at higher ZnO loadings can be ascribed to NP agglomeration and the increased exposure of oxygen-rich, hydrophilic ZnO sites [35], which promote water adhesion. At 15 wt%, partial aggregation slightly disturbs fiber uniformity and increases surface polarity, while at 20 wt% ZnO, excessive ZnO coverage leads to pronounced hydrophilic behavior and a partial transition from Cassie-Baxter to Wenzel wetting regimes [36]. Nevertheless, at ZnO concentrations of 10 wt% and 15 wt%, the WCAs remain relatively high, implying that the surfaces retain suitability for prospective self-cleaning applications. Even at 20 wt% ZnO loading, the WCA decreases to around 130°; however, the surface still exhibits hydrophobic characteristics, suggesting that the PVDF-HFP/ZnO nanofiber membranes maintain water repellency despite the increased ZnO content. Consequently, an optimal balance between surface roughness and hydrophobicity is achieved at 5 wt% ZnO, where the membrane exhibits the lowest surface free energy and the maximum WCA. These results confirm that a controlled ZnO dispersion enhances surface roughness without sacrificing hydrophobicity, which is a crucial factor for improving both the water-repellent and antibacterial performance of PVDF-HFP/ZnO nanofiber membranes.

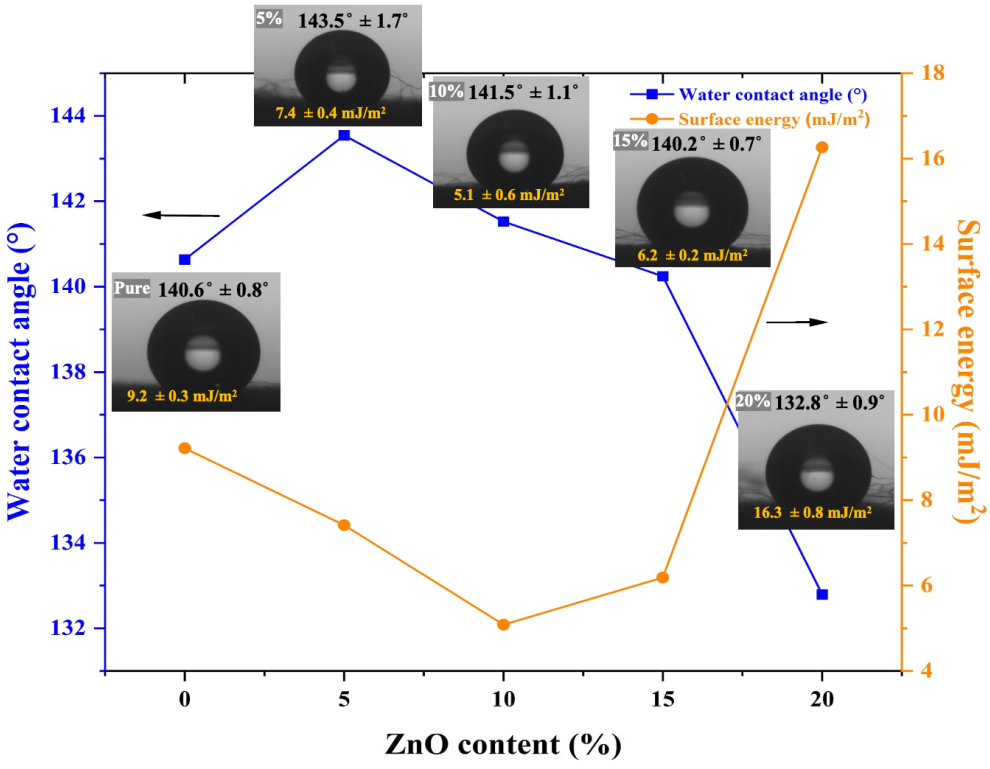

Figure 6 Water contact angle and surface energy of uncoated PVDF-HFP nanofibers and ZnO/PVDF-HFP composite nanofibers with varying ZnO contents (5%, 10%, 15%, and 20%).

FTIR analysis

FTIR spectroscopy plays a critical role in validating the presence of distinctive functional groups and elucidating their potential interactions within the complicated structure of polymeric materials [37]. As depicted in **Figure 7**, the FTIR spectra reveal the characteristic vibrational features of ZnO NPs, pristine PVDF-HFP powder, uncoated PVDF-HFP nanofibers, and ZnO/PVDF-HFP composite nanofibers with different ZnO NP loadings ranging from 5% to 20%. The vibrational peaks observed at approximately 876 and 1,033 cm^{-1} for pure ZnO NPs are due to the stretching vibrations of ZnO, confirming the formation of Zn-O bonds. In addition, the weak peaks around 1,446 cm^{-1} (C=C) and 1,634 cm^{-1} (C=O/C=C) may be attributed to hydroxyl groups on the ZnO surface. The broad absorption band centered near 3,438 cm^{-1} is assigned to O-H stretching vibrations, indicating the presence of surface-adsorbed water molecules or hydroxyl groups, which commonly arise from moisture adsorption on ZnO surfaces. The FTIR spectrum of the uncoated PVDF-HFP nanofibers exhibits characteristic bands at 840 cm^{-1}, corresponding to the β-phase, and at 764 cm^{-1}, associated with the α-phase, reflecting the presence of different crystalline phases of PVDF. In the ZnO/PVDF-HFP composite nanofibers, bands at 1,170, 1,074, and 1,234 cm^{-1} are consistent with those of the pristine polymer, although slight shifts and variations in intensity are noted. These changes are particularly evident in the region of 840 - 876 cm^{-1}, where overlap between the β-phase of PVDF and Zn-O vibrations occurs, as well as in the 1,000 - 1,250 cm^{-1} range attributed to C-F stretching and Zn-O bonding. Such spectral modifications indicate the existence of possible interactions or weak interfacial bonding between the Zn-O groups of ZnO NPs and the $-CF_2$ groups of the PVDF-HFP matrix [38]. Importantly, these interactions do not disrupt the primary polymer backbone, suggesting effective incorporation of ZnO within the polymer matrix. Furthermore, increasing the ZnO amount from 5% to 20% results in a gradual enhancement of Zn-O peak intensities, verifying the gradual and successful incorporation of ZnO NPs. Meanwhile, a modest increase in the absorption intensity associated with the β-phase (~840 cm^{-1}) is noted, implying that ZnO NPs likely act as nucleating agents that promote the phase transformation of PVDF from α- to β-phase [39]. The β-phase of PVDF is characterized by an all-trans (TTTT) planar zigzag chain conformation, in which the molecular dipoles are aligned parallel in the same direction, resulting in a large net dipole moment and strong spontaneous polarization. In contrast, the α-phase adopts a trans-gauche-trans-gauche′ (TGTG′) conformation with antiparallel dipole arrangement, which significantly reduces the overall polarity. Consequently, the β-phase exhibits superior electroactive behavior, including enhanced piezoelectric, pyroelectric, ferroelectric, and dielectric properties, making it highly desirable for electroactive and sensing applications.

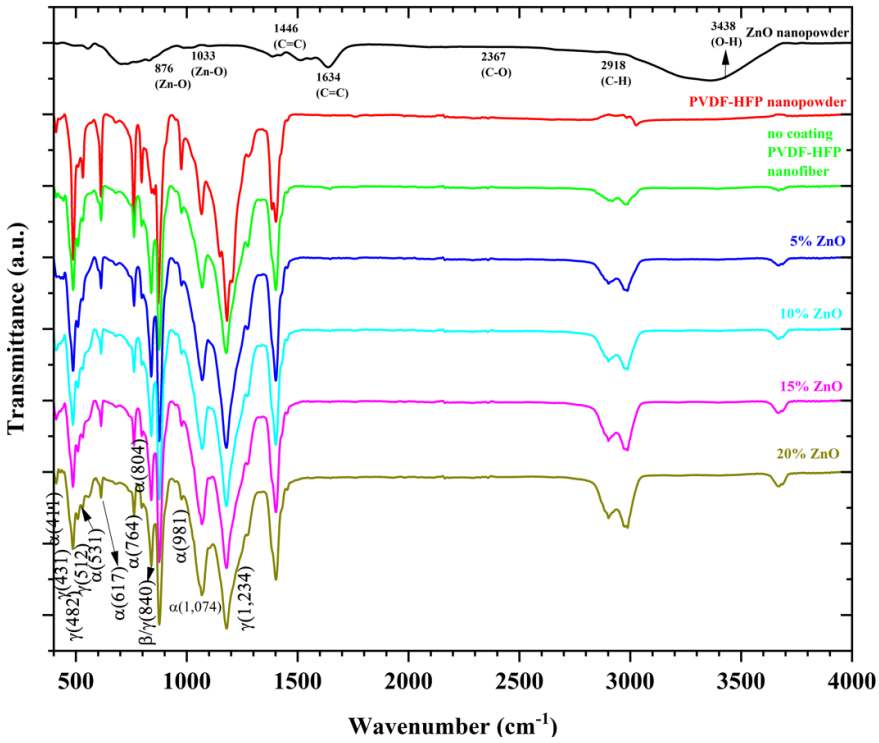

Figure 7 FTIR spectra of ZnO nanoparticles, PVDF-HFP powder, uncoated PVDF-HFP nanofibers, and ZnO/PVDF-HFP composite nanofibers with ZnO contents ranging from 5% to 20%.

XRD analysis

X-ray diffraction (XRD) is a widely used analytical technique commonly employed to investigate the crystal structure, phase composition, and average crystallite size of nanomaterials. It provides fundamental information about the atomic arrangement and phase purity of synthesized materials, which is crucial for understanding their physicochemical properties and functional performance in various applications. The XRD pattern of the as-synthesized ZnO powder is presented in **Figure 8**. Distinct diffraction peaks observed at 2θ values of approximately 31.7°, 34.4°, 36.2°, 47.5°, 56.6°, 62.8°, 66.3°, 68°, and 69.1° correspond to the (100), (002), (101), (102), (110), (103), (200), (112), and (201) crystallographic planes, respectively. These reflections closely match the standard hexagonal wurtzite structure of ZnO (JCPDS 36-1451), confirming the formation of a single-phase material without any detectable impurities such as metallic Zn or $Zn(OH)_2$ [40]. The presence of sharp and intense diffraction peaks indicates the high degree of crystallinity of the ZnO NPs. Notably, the most intense diffraction peak at $2\theta = 36.2°$ is assigned to the (101) plane, which is a characteristic reflection of wurtzite ZnO.

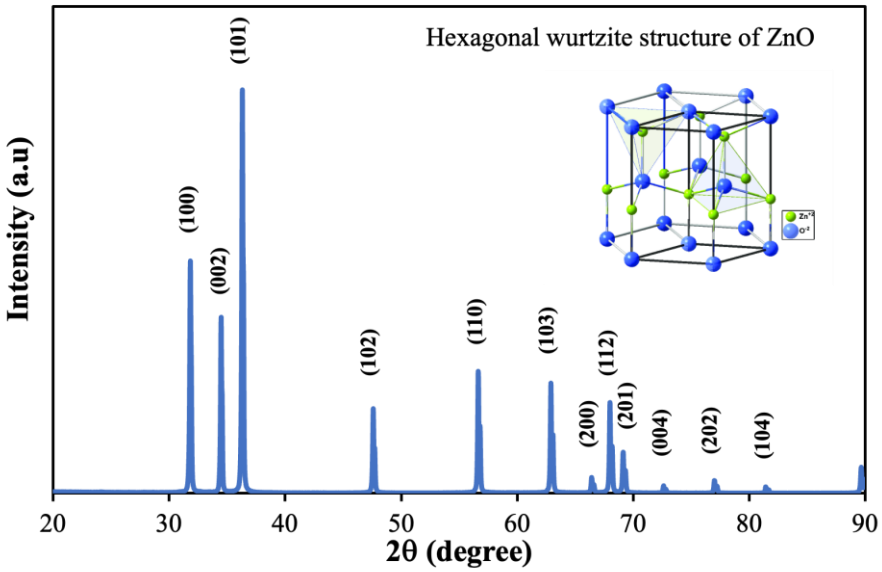

Figure 8 X-ray diffraction patterns displaying (hkl) values are presented for green synthesized ZnO NPs.

The XRD patterns of pristine ZnO nanopowder, PVDF-HFP powder, uncoated PVDF-HFP nanofibers, and ZnO-coated PVDF-HFP nanofibers containing different ZnO content (5 wt% - 20 wt%) are shown in **Figure 9**. The XRD pattern of the uncoated PVDF-HFP nanofibers displays peaks at 17.7°, 20.4°, 26.2°, and 36.9°, which correspond to the (100), (110)/(200), (021), and (022) planes, respectively. These reflections are attributed to the α-, β-, and γ-phase of PVDF-HFP, as reported in the literature [41]. The prominent peak around 20.4° is indicative of the β-phase, which is associated with a strong dipole moment and superior ferroelectric behavior, whereas the peak at nearly 18.3° represents the α-phase. The diffraction signal appearing at 36.9° is related to the γ-phase of the polymer. After coating with ZnO NPs, additional peaks emerge in the XRD patterns of the coated nanofibers, confirming the successful incorporation of crystalline ZnO within the PVDF-HFP matrix. No additional impurity peaks are detected, indicating that ZnO maintains its hexagonal wurtzite structure and undergoes no chemical degradation during the coating process. Furthermore, the characteristic peaks of PVDF-HFP remain clearly distinguishable, demonstrating strong interfacial compatibility between PVDF-HFP and ZnO. This behavior is ascribed to the electrostatic interactions and possible hydrogen bonding between the F atom of the -CF_2- groups in PVDF-HFP and the surface hydroxyl groups of ZnO NPs [42,43].

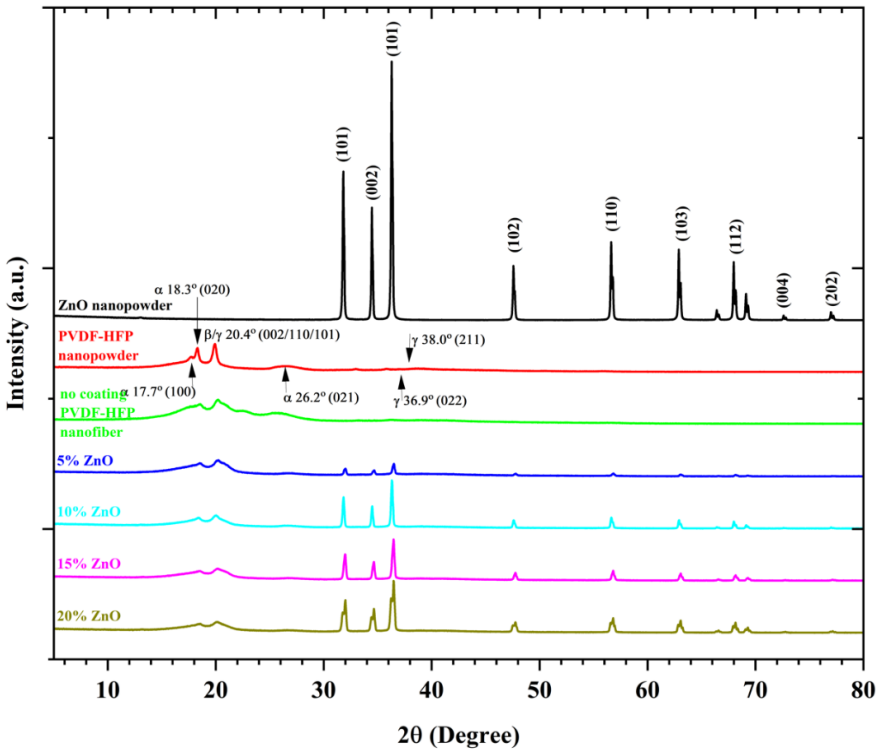

Figure 9 XRD patterns of ZnO nanoparticles, PVDF-HFP powder, uncoated PVDF-HFP nanofibers, and ZnO/PVDF-HFP composite nanofibers with ZnO contents ranging from 5% to 20%.

Table 1 Crystallinity of ZnO NPs, PVDF-HFP powder, uncoated PVDF-HFP nanofibers, and ZnO/PVDF-HFP composite nanofibers with varying ZnO contents (5 wt% - 20 wt%), calculated from XRD data using the ratio of net peak intensity to total diffraction intensity.

Sample	Sum of net intensity		Crystallinity (%)
	Peak (cts)	Total (cts)	
ZnO NPs	2294954.00	2538405.00	90.41
PVDF-HFP powder	321141.70	2362537.00	13.59
Uncoated PVDF-HFP nanofibers	301329.10	1200454.00	25.10
5 wt% ZnO/PVDF-HFP nanofibers	308480.40	1223402.00	25.21
10 wt% ZnO/PVDF-HFP nanofibers	550733.60	1221214.00	45.10
15 wt% ZnO/PVDF-HFP nanofibers	584497.60	1279850.00	45.67
20 wt% ZnO/PVDF-HFP nanofibers	894594.50	1615040.00	55.39

Table 1 presents the crystallinity values of ZnO NPs, PVDF-HFP powder, uncoated PVDF-HFP nanofibers, and ZnO/PVDF-HFP composite nanofibers containing 5 wt% - 20 wt% ZnO. The pristine ZnO NPs show the highest crystallinity of 90.41%, which reflects their well-ordered hexagonal wurtzite structure, as evidenced by intense, and sharp diffraction peaks. In contrast, the PVDF-HFP powder exhibits a markedly lower crystallinity of 13.59%, indicating a predominantly amorphous phase with limited chain ordering and the coexistence of α-, β-, and γ-phases [44]. Following electrospinning, the crystallinity of the uncoated PVDF-HFP nanofibers increases to 25.10%. This improvement is mainly attributed to the stretching and orientation of molecular chains during the electrospinning process, which enhances the formation of the electroactive β-phase responsible for its ferroelectric behavior [45]. The progressive increase in crystallinity observed in the ZnO/PVDF-HFP composite nanofibers suggests that ZnO nanoparticles act as

nucleating agents, promoting molecular ordering and β-phase evolution within the polymer matrix through interfacial interactions between ZnO and PVDF-HFP chains. The incorporation of ZnO NPs results in a progressive enhancement in the crystallinity of the nanofibers, with values reaching 25.21% at 5 wt% ZnO, 45.10% at 10 wt% ZnO, 45.67% at 15 wt% ZnO, and 55.39% at 20 wt% ZnO. This continuous increase suggests that ZnO effectively acts as a nucleating agent, promoting better alignment of PVDF-HFP polymer chains. Specifically, interfacial interactions between the F atoms of PVDF-HFP (-CF_2 groups) and the surface hydroxyl groups of ZnO NPs encourage crystal growth and structural ordering. The observed enhancement in crystallinity confirms the successful dispersion and addition of ZnO with the PVDF-HFP matrix, which corresponds well with the stronger ZnO diffraction peaks observed in XRD patterns. In general, increased crystallinity is associated with improved thermal stability, enhanced mechanical strength, and stronger interfacial bonding between the polymer matrix and the inorganic filler. However, excessive ZnO concentration can induce partial NP aggregation, which in turn restricts polymer chain mobility. Therefore, a ZnO content of approximately 10% - 15% is identified as optimal, achieving a balance between enhanced crystallinity and overall material performance.

Thermal properties

The thermal behavior of the ZnO/PVDF-HFP composite nanofibers, ZnO nanopowder, and the corresponding reference samples was analyzed using TGA coupled with derivative thermogravimetric (DTG) analysis (**Figure 10)**. The TGA curves illustrate the variation in weight loss (%) as a function of temperature, while the DTG curves highlight the corresponding decomposition rates. The ZnO nanopowder exhibits excellent thermal stability, maintaining nearly its entire mass up to 700 °C, confirming the chemically inert and thermally stable nature of ZnO NPs [46]. Such high stability provides a reinforcing effect in the nanocomposite by serving as an effective thermal barrier that delays the thermal degradation of the polymer matrix. In contrast, pure PVDF-HFP powder displays a distinct single-step degradation process, with decomposition initiating at around 430 °C and reaching a maximum rate near 470 °C. This behavior is related to dehydrofluorination reactions and the subsequent scission of the polymer backbone [47]. The sharp weight loss observed is typical for PVDF-based polymers and is associated with the thermal breakdown of -CH_2 and -CF_2 chains, releasing gaseous products such as hydrogen fluoride and carbonaceous residues. Notably, the uncoated PVDF-HFP nanofiber demonstrates marginally enhanced thermal resistance compared with its powdered counterpart. This is primarily attributed to the highly oriented fibrous morphology and increased crystallinity induced during electrospinning. Such structural orientation restricts molecular mobility, thereby delaying the onset of thermal degradation.

Furthermore, the incorporation of ZnO NPs as a surface coating markedly improves the thermal stability of the ZnO/PVDF-HFP nanofiber composites. Both the onset decomposition temperature (T_o) and the temperature corresponding to maximum mass loss (T_{max}) increase progressively with increasing ZnO loading, indicating improved thermal resistance. Composites containing 5 wt% and 10 wt% ZnO show slower degradation and reduced weight loss compared with the uncoated nanofibers, while those with 15 wt% and 20 wt% ZnO achieve the highest thermal stability among all samples. This improvement is mainly due to: (i) strong interfacial bonding between ZnO NPs and PVDF-HFP chains, which inhibits chain scission; (ii) the high thermal conductivity and heat-absorbing properties of ZnO, enabling more efficient redistribution of thermal energy; and (iii) the formation of a compact char layer during degradation that serves as an insulating barrier to oxidative decomposition [48]. Moreover, the enhanced thermal performance strongly correlates with the increase in crystallinity, as evidenced by XRD analysis. With the ZnO content increased from 5 wt% to 20 wt%, the crystallinity of the PVDF-HFP nanofibers rise markedly from 25.21% to 55.39%. An elevated degree of crystallinity reflects improved molecular ordering and a lower proportion of amorphous regions, which are typically more susceptible to thermal degradation. The more ordered crystalline domains require greater energy to decompose, thereby increasing the decomposition temperature and improving overall stability. In addition, ZnO serves as a nucleating agent, promoting the growth of the electroactive β-phase of PVDF-HFP, which is characterized by strong dipole alignment and superior

thermal endurance [49]. This structural reinforcement further supports the observed improvements in the TGA-DTG results. At a high ZnO concentration of 20 wt%, a slight reduction in thermal resistance is observed despite its high crystallinity. This can be attributed to partial agglomeration of ZnO NPs, which weakens interfacial adhesion and causes localized heat accumulation. Nevertheless, the composite still retains a high residual weight at 700 °C, corresponding to the stable ZnO component. This outcome confirms the successful incorporation of the inorganic phase within the nanofiber matrix and demonstrates its excellent thermal durability.

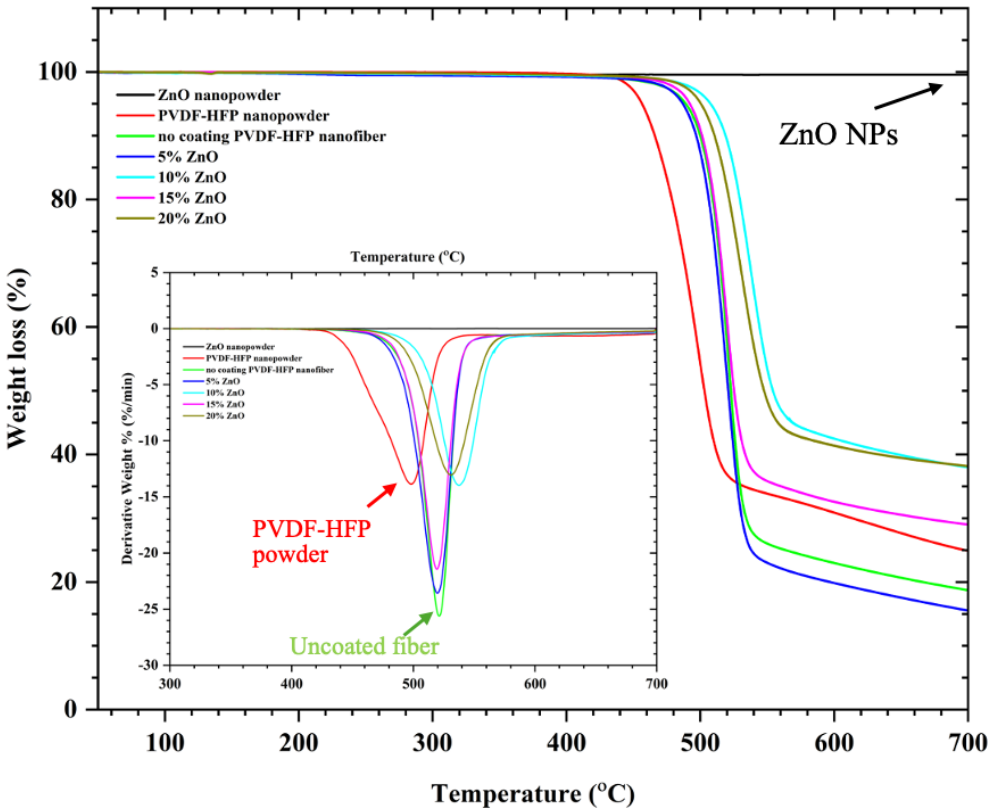

Figure 10 TGA and DTG thermograms of ZnO nanopowder, PVDF-HFP nanopowder, uncoated PVDF-HFP nanofiber, and ZnO/PVDF-HFP composite nanofibers with varying ZnO contents (5%, 10%, 15%, and 20%).

Mechanical properties

The mechanical behavior of uncoated PVDF-HFP nanofibers and ZnO/PVDF-HFP composite nanofibers with varying ZnO content (5% - 20%) was investigated through tensile testing, with the results presented in **Figure 11** and summarized in **Table 2**. The uncoated PVDF-HFP nanofibers exhibit a tensile strength of 2.62 ± 0.13 MPa and an elongation at break of 271.7 ± 15.2%, demonstrating a balance between flexibility and moderate strength. This behavior is characteristic of electrospun polymer fibers, which typically exhibit relatively high chain mobility and reduced crystallinity. During electrospinning, the polymer jet experiences rapid elongational stretching and ultrafast solvent evaporation under a high electric field, restricting the time required for polymer chains to reorganize into thermodynamically stable crystalline domains. Consequently, electrospun fibers generally possess a higher amorphous fraction, increased free volume, and reduced chain packing density compared with bulk polymers. Furthermore, the interconnected porous nanofibrous structure facilitates segmental chain motion and enhances polymer chain flexibility, thereby contributing to increased chain mobility. Upon the incorporation of ZnO NPs, the mechanical response of the nanofibers changes considerably. In particular, the 5 wt% ZnO/PVDF-HFP composite exhibits a significant decrease in tensile strength to 1.35 ± 0.07 MPa,

accompanied by an increase in elongation at break to 335.6 ± 15.5%. This behavior suggests that a small amount of ZnO NPs functions as a plasticizing agent, increasing inter-fiber slippage and ductility by weakening intermolecular interactions between polymer chains. In addition, dispersed NPs introduce minor imperfections within the matrix, which facilitate localized deformation before fracture, thereby enhancing stretchability.

At moderate ZnO contents of 10 wt% and 15 wt%, the tensile strength is restored and is further increased to 2.41 ± 0.04 MPa and 2.48 ± 0.14 MPa, respectively, whereas the elongation at break gradually declines to 253.9 ± 33.8% and 241.2 ± 17.4%, respectively. This improvement in mechanical strength is primarily due to the formation of strong interfacial bonding between the ZnO NPs and the PVDF-HFP matrix, resulting from electrostatic interactions between the F-containing groups (–CF_2–) of PVDF-HFP and the hydroxyl sites on the ZnO surface. Moreover, the XRD analysis reveals a pronounced increase in crystallinity, rising from 25.10% for the uncoated fiber to 45.10% and 45.67% for 10 wt% and 15 wt% ZnO composites, respectively. This contributes to more efficient load transfer and molecular alignment under stress. The increased ordering and chain packing provide greater stiffness and resistance to deformation, leading to improved tensile strength at the expense of slight flexibility loss. When the ZnO loading is increased to 20 wt%, the tensile strength reaches 2.66 ± 0.34 MPa, remaining comparable to that of the uncoated nanofiber; however, the elongation at break decreases further to 215.3 ± 18.9%. This additional reduction in ductility is ascribed to ZnO NP aggregation, which introduces micro-defects and stress concentration points within the nanofiber network [50]. These agglomerates hinder uniform stress distribution and restrict polymer chain movement, resulting in brittle fracture behavior. Although higher ZnO content enhances crystallinity (up to 55.39%), excessive filler addition can compromise the overall flexibility of the composite owing to reduced polymer-polymer contact and increased particle-particle interaction [51]. Mechanical analysis reveals that a ZnO loading in the range of 10 wt% - 5 wt% achieves an optimal compromise between tensile strength and flexibility. These trends are consistent with the SEM and XRD findings, confirming that improved interfacial adhesion, uniform particle dispersion, and increased crystallinity collectively govern the mechanical reinforcement of ZnO/PVDF-HFP nanofibers. Consequently, the optimized compositions are suitable for applications requiring both mechanical robustness and functional surface properties, including self-cleaning and protective membrane systems.

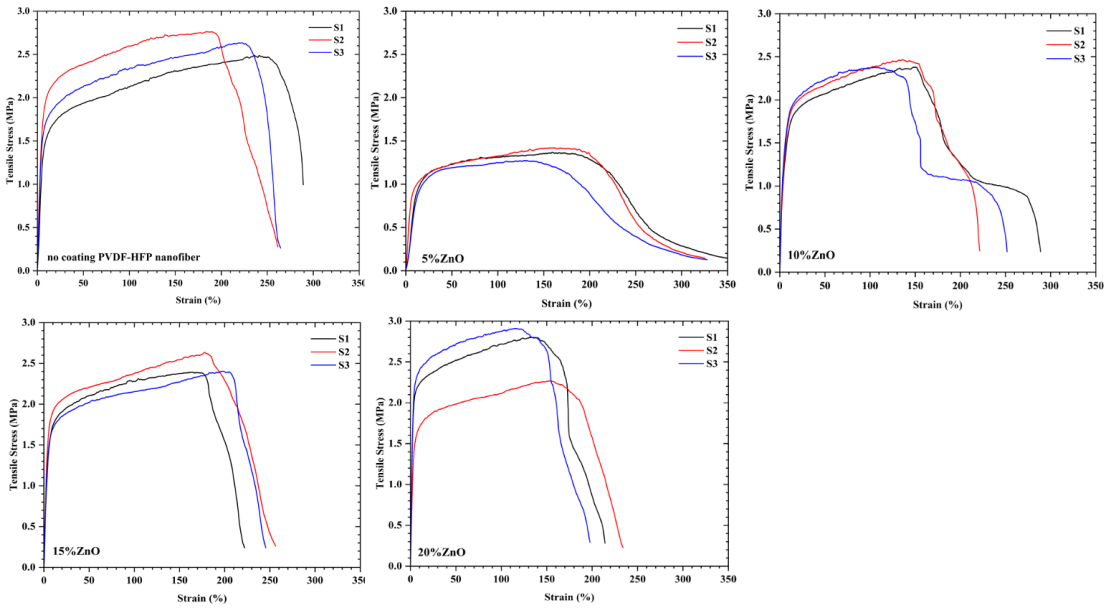

Figure 11 Stress-strain curves of uncoated PVDF-HFP nanofibers, and ZnO/PVDF-HFP composite nanofibers with ZnO contents ranging from 5% to 20%.

Table 2 Mechanical properties of uncoated PVDF-HFP nanofibers and ZnO/PVDF-HFP composite nanofibers with ZnO contents ranging from 5 wt% to 20 wt%.

PVDF-HFP Nanofibers samples	Tensile strength (MPa)	Elongation at break (%)
Uncoated	2.62 ± 0.13	271.7 ± 15.2
5% ZnO	1.35 ± 0.07	335.6 ± 15.5
10% ZnO	2.41 ± 0.04	253.9 ± 33.8
15% ZnO	2.48 ± 0.14	241.2 ± 17.4
20% ZnO	2.66 ± 0.34	215.3 ± 18.9

Antibacterial activity analysis

The antimicrobial activity of uncoated PVDF-HFP nanofibers and ZnO/PVDF-HFP composite nanofibers containing various ZnO contents (5 - 20 wt%) was studied using the disc diffusion method. Pristine PVDF-HFP nanofibers serve as the control. The average diameters of the inhibition zones against *S. aureus* and *S. epidermidis* are summarized in **Table 3**. No inhibition zones are observed for the original and alcohol-soaked PVDF-HFP nanofibers. In contrast, the inhibition zone size increases with increasing ZnO loading, suggesting a strong dependence of antibacterial efficiency on the concentration of ZnO NPs incorporated into the polymer matrix. For *S. aureus*, the inhibition zone measures 17.10 ± 1.59 mm at 5 wt% ZnO, slightly decreases to 12.85 ± 0.41 mm and 13.50 ± 0.55 mm at 10 wt% and 15 wt% ZnO, respectively, and then increases again to 15.00 ± 1.41 mm at 20 wt% ZnO. A similar trend is recorded for *S. epidermidis*, with inhibition zone diameters of 13.00 ± 2.37 mm, 14.80 ± 0.41 mm, 14.15 ± 0.55 mm, and 13.95 ± 1.10 mm at ZnO loadings of 5 wt%, 10 wt%, 15 wt%, and 20 wt%, respectively. For S. *aureus,* the 5 wt% ZnO/PVDF-HFP composite exhibited the largest inhibition zone, whereas for S. *epidermidis,* the antibacterial activity slightly increased at moderate ZnO loadings. Overall, ZnO incorporation significantly enhanced the antibacterial activity compared with uncoated PVDF-HFP nanofibers. This enhanced performance can be attributed to the higher surface exposure of ZnO NPs, leading to the increased generation of ROS, such as hydroxyl radicals (•OH) and superoxide anions (O_2•$^-$), which can damage bacterial cell membranes, proteins, and nucleic acids. Moreover, the release of Zn^{2+} ion from ZnO NPs can penetrate through the bacterial cell wall, disrupting enzyme activity and essential metabolic processes [52,53]. The synergistic action of oxidative stress and ionic disruption is particularly effective against *S. aureus* and *S. epidermidis*, as these Gram-positive bacteria possess thick peptidoglycan layers that are susceptible to ROS-mediated damage. The enhanced antibacterial activity of the ZnO/PVDF-HFP composite nanofibers can be attributed to the well-established antibacterial mechanisms of ZnO nanoparticles, particularly reactive oxygen species (ROS) generation and Zn^{2+} ion release. ZnO nanoparticles are known to generate ROS, including hydroxyl radicals (•OH), superoxide anions (O_2•$^-$), and hydrogen peroxide (H_2O_2), which induce oxidative stress and damage essential bacterial cellular components such as cell membranes, proteins, and nucleic acids. In addition, partial dissolution of ZnO in aqueous environments may release Zn^{2+} ions that interact with bacterial cell membranes, disrupt membrane integrity, interfere with intracellular enzymatic systems, and inhibit vital metabolic activities [54,55] (Elmayah *et al*., [54]; Popova *et al*., [55]). The improved antibacterial performance observed with increasing ZnO loading in this study is consistent with these previously reported mechanisms. In addition, our previous work [56] (Porrawatkul *et al*., [56]) experimentally verified ROS production using probe-based techniques and demonstrated a direct relationship between ROS generation and antibacterial efficiency. Although ROS generation and Zn^{2+} ion release were not directly quantified in the present work, the observed antibacterial behavior reasonably suggests the synergistic contribution of ROS-mediated oxidative stress and Zn^{2+} ion release. Furthermore, the electrospun nanofibrous morphology provides a high specific surface area, promoting effective contact between ZnO nanoparticles and bacterial cells, thereby further enhancing antibacterial activity. Direct ROS quantification and Zn^{2+} ion leaching analysis will be

considered in future work. Clear inhibition zones can be observed surrounding the samples (**Figure 12**), indicating that the active components released from the nanofiber composites effectively inhibit bacterial growth.

Table 3 Zone of inhibition (mm) of uncoated PVDF-HFP nanofibers and ZnO/PVDF-HFP composite nanofibers.

Samples	Zone of inhibition (mm)	
	S. aureus	***S. epidermidis***
Original PVDF-HFP nanofiber	ND	ND
Alcohol-soaked nanofiber	ND	ND
5 wt% ZnO	17.10 ± 1.59	13.00 ± 2.37
10 wt% ZnO	12.85 ± 0.41	14.80 ± 0.41
15 wt% ZnO	13.50 ± 0.55	14.15 ± 0.55
20 wt% ZnO	15.00 ± 1.41	13.95 ± 1.10

ND = Not detected.

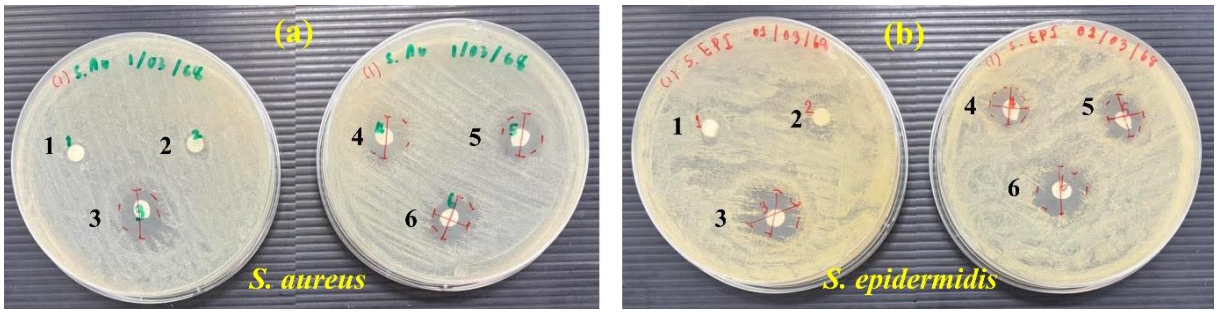

Figure 12 Antibacterial activity against (a) *S. aureus* and (b) *S. epidermidis* of 1. Original PVDF-HFP nanofiber, 2. Nanofiber and ZnO/PVDF-HFP composite nanofibers containing of 3. ZnO 5%, 4 ZnO 10%, 5 ZnO 10%, and 6 ZnO 20%.

The incorporation of ZnO NPs onto PVDF-HFP nanofibers forms a highly stable and multifunctional composite exhibiting exceptional antibacterial and self-cleaning properties. The interaction between the ZnO phase and the fluorinated polymer improves interfacial adhesion, surface functionality, and biological activity. The stable addition of ZnO onto electrospun PVDF-HFP nanofibers is accomplished by a combination of chemical bonding and physical entrapment. Surface hydroxyl groups on ZnO NPs interact with the fluorinated segments of PVDF-HFP via hydrogen bonding, electrostatic attraction, and coordination bonds (Zn–F or Zn–O–C). These connections establish a covalent network that holds the NPs strongly to the nanofiber surfaces [57]. Furthermore, the porous morphology and high surface area of the electrospun PVDF-HFP matrix facilitate the physical embedding of ZnO NPs within the nanofibers, resulting in a durable and uniform coating. Morphologically, the deposition of ZnO NPs imparts hierarchical nanoscale roughness to the PVDF-HFP surface, thus increasing surface energy and enhancing wettability. This structural modification transforms the originally hydrophobic PVDF-HFP into a hydrophilic and light-scattering surface. The improved surface roughness further supports strong water spreading and facilitates pollutant removal, forming the foundation for self-cleaning performance. Upon UV irradiation, ZnO acts as a semiconductor photocatalyst, generating ROS, such as •OH and O_2•$^-$, which decompose microbial residues [58]. Furthermore, the strong anchoring of ZnO within the PVDF-HFP matrix ensures a stable and long-lasting antibacterial effect, minimizing NP leaching an essential requirement for both biomedical and environmental safety. The formation and functional behavior of ZnO/PVDF-HFP composite nanofibers are shown in **Figure 13**. Although

the antibacterial activity of ZnO-coated PVDF-HFP nanofibers was systematically investigated in comparison with uncoated PVDF-HFP membranes, the present study did not include standard antibiotic positive controls or pure ZnO nanoparticle samples. Nevertheless, previous studies have consistently demonstrated that ZnO nanoparticles exhibit strong antibacterial activity through reactive oxygen species generation and Zn^{2+} ion release mechanisms. Future investigations will focus on comparative antibacterial studies involving standard antibiotic controls and pure ZnO nanoparticles to further quantify the individual contribution of ZnO and the synergistic effects arising from the nanofibrous composite structure.

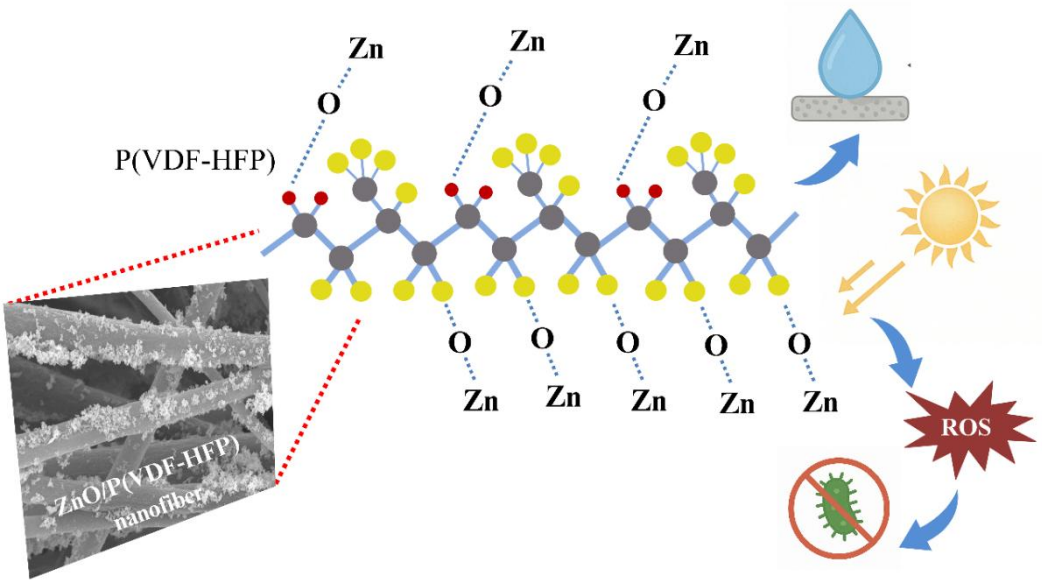

Figure 13 Formation and functional behavior of ZnO/PVDF-HFP composite nanofibers.

Conclusions

Electrospun PVDF-HFP nanofiber membranes coated with ZnO NPs were successfully fabricated and systematically characterized to evaluate their potential as multifunctional air-filtration materials. The incorporation of ZnO NPs significantly enhanced the crystallinity, surface morphology, and thermal stability of the nanofibers, while maintaining excellent mechanical flexibility. Among the prepared samples, the 5 wt% ZnO-coated membrane displayed the highest hydrophobicity, exhibiting a WCA of 143.5°, indicative of superior self-cleaning properties. Higher ZnO content further improved structural order and interfacial bonding, contributing to improved mechanical strength and heat resistance up to 700 °C. Antibacterial assays confirmed strong inhibitory activity against *S. aureus* and *S. epidermidis*, showing inhibition zones of 17.10 ± 1.59 mm (5 wt% ZnO) and 14.80 ± 0.41 mm (10 wt% ZnO), respectively. These findings demonstrated that ZnO NPs effectively generated ROS and released Zn^{2+} ions, disrupting bacterial membranes and suppressing microbial proliferation. Therefore, the ZnO/PVDF-HFP nanofiber membranes exhibited a unique combination of hydrophobicity, mechanical durability, and potent antibacterial efficiency, highlighting their potential for self-cleaning, high-performance air-filtration, and protective mask applications. Future work should focus on optimizing NP dispersion, assessing membrane reusability, and integrating photocatalytic properties to further enhance environmental protection and air-purification performance.

Acknowledgments

This research was financially supported by the Science, Mathematics, Technology, and Environment (SMTE) Program, Benjamarachutit School, under the Memorandum of Understanding (MOU) between Nakhon Si Thammarat Rajabhat University (NSTRU), Nakhon Si Thammarat 80280, Thailand and Benjamarachutit School, Nakhon Si Thammarat, Thailand. The authors would like to express their sincere gratitude to Nakhon Si Thammarat Rajabhat University

for its essential support and facilitation of this work. Special thanks are extended to the Division of Physical Science (Physics), Faculty of Science, Prince of Songkla University, for providing instrumental and technical assistance. The authors also acknowledge the faculty members and staff of Nakhon Si Thammarat Rajabhat University for their continuous encouragement and valuable resources throughout the course of this study.

Data Availability Statement

The processed data required to reproduce these findings is available from the authors upon reasonable request.

Declarations Statement

During the preparation of this work, the authors used ChatGPT solely for grammar checking. After using this tool, the authors thoroughly reviewed and edited the content as necessary and take full responsibility for the final version of the manuscript.

Author contributions

Paweena Porrawatkul: Investigation, Formal analysis, Writing original draft, Writing review & editing, Conceptualization, Data curation; **Sirikun Pethuan:** Methodology, Conceptualization; **Jureeporn Yuennan:** Methodology, Formal analysis, Writing original draft, Writing review & editing, Conceptualization, Data curation; **Nikruesong Tohluebaji:** Investigation, Formal analysis, Conceptualization, Writing original draft, Writing – review & editing; **Ponkanok Dawan:** Investigation, Formal analysis, Writing original draft; **Pitsinee Supakitanan:** Investigation, Formal analysis, Writing original draft; **Arachaporn Vijara:** Investigation, Formal analysis, Writing original draft; **Ratchanewan Siri:** Investigation; Nantakan Muensit: Supervision; Chatchai Putson: Investigation; **Thammarong Eadkhong:** Supervision; **Phongpichit Channuie:** Supervision.

References

[1] WWF Leung and Q Sun. Charged PVDF multilayer nanofiber filter in filtering simulated airborne novel coronavirus (COVID-19) using ambient nano-aerosols. *Separation and Purification Technology* 2020; **245**, 116887.

[2] N Chen, M Zhou, X Dong, J Qu, F Gong, Y Han, Y Qiu, J Wang, Y Liu, Y Wei, J Xia, T Yu, X Zhang and L Zhang. Epidemiological and clinical characteristics of 99 cases of 2019 novel coronavirus pneumonia in Wuhan, China: A descriptive study. *The Lancet* 2020; **395(10223)**, 507-513.

[3] S Karimzadeh, R Bhopal and NT Huy. Review of infective dose, routes of transmission and outcome of COVID-19 caused by the SARS-COV-2: Comparison with other respiratory viruses. *Epidemiol Infect* 2021; **149**, e96.

[4] AL Rasmussen, K Escandón and SV Popescu. Facial Masking for Covid-19. *The New England Journal of Medicine* 2020; **383(21)**, 2092-2094.

[5] M Liang, L Gao, C Cheng, Q Zhou, JP Uy, K Heiner and C Sun. Efficacy of face mask in preventing respiratory virus transmission: A systematic review and meta-analysis. *Travel Medicine and Infectious Disease* 2020; **36**, 101751.

[6] JAT Ruiz, A Vitale and L Pattelli. Solvent role for the electrospinning of PVDF-HFP nanofibrous coatings for passive radiative cooling applications. *The European Physical Journal Conferences* 2024; **309**, 13009.

[7] S Aghayari. PVDF composite nanofibers applications. *Heliyon* 2022; **8(11)**, e11620.

[8] P Filip, J Zelenkova and P Peer. Electrospinning of a copolymer PVDF-*co*-HFP solved in DMF/Acetone: Explicit relations among viscosity, polymer concentration, DMF/Acetone ratio and mean nanofiber diameter. *Polymers* 2021; **13(19)**, 3418.

[9] KČ Barabaszová, S Holešová, M Hundáková, K Hrabovská, L Plesník, D Kimmer, K Joszko, B Gzik-Zroska and M Basiaga. Antimicrobial PVDF nanofiber composites with the ZnO - vermiculite - chlorhexidine based nanoparticles and their tensile properties. *Polymer Testing* 2021; **103**, 107367.

[10] F Russo, C Ursino, E Avruscio, G Desiderio, A Perrone, S Santoro, F Galiano and A Figoli. Innovative Poly (Vinylidene Fluoride) (PVDF) electrospun nanofiber membrane preparation using DMSO as a low toxicity solvent. *Membranes* 2020; **10(3)**, 36.

[11] D Abbas, MS Mu'min, M Bonanno, S Thiele and T Böhm. Active solution heating and cooling in electrospinning enabling spinnability from various solvents. *Journal of Applied Polymer Science* 2022; **139**, e52730.

[12] K Liu, Z Chen, M Guan, J Jin, C Ren, S Gu and W Zhang. High-performance coupled nanogenerators based on electrospun porous PU@PVDF-ZnO nanofibers with core–shell structure. *Advanced Engineering Materials* 2025; **27(19)**, 2500549.

[13] RK Singh, SW Lye and J Miao. Holistic investigation of the electrospinning parameters for high percentage of β-phase in PVDF nanofibers. *Polymer* 2021; **214**, 123366.

[14] H Parangusan, D Ponnamma and MAA Al-Maadeed. Stretchable electrospun PVDF-HFP/Co-ZnO nanofibers as piezoelectric nanogenerators. *Scientific Reports* 2018; **8(1)**, 754.

[15] J Chen, J Fan, M Livojevic, M Gupta, T Tang and C Ayranci. Enhancing piezoelectric properties of PVDF-HFP composite nanofibers with cellulose nanocrystals. *Materials Today Communications* 2024; **39**, 108872.

[16] B Chamam, RB Dassi, J Abderraouf, JP Mericq, C Faur, I Trabelsi, LE Mir and M Heran. Incorporation of Ag-ZnO nanoparticles into PVDF membrane formulation to enhance dye retention, permeability, and antibacterial properties. *Polymers* 2025; **17(9)**, 1269.

[17] Y Niu, Q Jia, S Yan, J Zhang, and L Han. Co-electrospun PU–PVDF/TiO_2 nanofiber membranes: A multifunctional strategy for durable, antibacterial, and low-resistance air filters. *Journal of Materials Science* 2025; **60**, 20384-20395.

[18] VR Lebaka, P Ravi, MC Reddy, C Thummala and TK Mandal. Zinc oxide nanoparticles in modern science and technology: Multifunctional roles in healthcare, environmental remediation, and industry. *Nanomaterials* 2025; **15(10)**, 754.

[19] S Baskoutas and G Bester. Conventional optics from unconventional electronics in ZnO quantum dots. *The Journal of Physical Chemistry C* 2010; **114(20)**, 9301-9307.

[20] S Dey, Dl Mohanty, N Divya, V Bakshi, A Mohanty, D Rath, S Das, A Mondal, S Roy and R Sabui. A critical review on zinc oxide nanoparticles: Synthesis, properties and biomedical applications. *Intelligent Pharmacy* 2025; **3(1)**, 53-70.

[21] E Rincon-Suarez, JM Mozo, A Romero-López, S Alcántara-Iniesta, FJ Flores-Ruiz and LE Serrano. Structural, optical and electrical properties of ZnO thin films deposited in the plane direction (002) by ultrasonic spray pyrolysis using nitrogen as carrier gas. *Materials Science and Engineering: B* 2025; **320**, 118430.

[22] J Lu, P Dong, Y Zhao, Y Zhao and Y Zeng. 3D printing of TPMS structural ZnO ceramics with good mechanical properties. *Ceramics International* 2021; **47(9)**, 12897-12905.

[23] SR Kelly, X Shi, S Back, L Vallez, SY Park, S Siahrostami, X Zheng and JK Nørskov. ZnO As an active and selective catalyst for electrochemical water oxidation to hydrogen peroxide. *ACS Catalysis* 2019; **9(5)**, 4593-4599.

[24] L Foster, JA Foppiani, H Xun, D Lee, B Utz, AH Alvarez, MJ Domingo-Escobar, IC Taritsa, D Gavlasova, TC Lee, GJ Lin, U Choudry and SJ Lin. Zinc in dermatology: Exploring its emerging role in enhancing botulinum toxin formulations and clinical efficacy. *Current Issues in Molecular Biology* 2024; **46(11)**, 12088-12098.

[25] N Padmavathy and R Vijayaraghavan. Enhanced bioactivity of ZnO nanoparticles-an antimicrobial study. *Science and Technology of Advanced Materials* 2008; **9(3)**, 035004.

[26] XQ Zhou, Z Hayat, DD Zhang, MY Li, S Hu, Q Wu, YF Cao and Y Yuan. Zinc oxide nanoparticles: Synthesis, characterization, modification, and applications in food and agriculture. *Processes* 2023; **11(4)**, 1193.

[27] R Rohani, NSF Dzulkharnien, NH Harun and IA Ilias. Green approaches, potentials, and applications of Zinc Oxide nanoparticles in surface coatings and films. *Bioinorganic Chemistry and Applications* 2022; **2022**, 3077747.

[28] AEA Yagoub, GM Al-Shammari, LN Al-Harbi, P Subash-Babu, R Elsayim, MA Mohammed, MA Yahya and SZA Fattiny. Antimicrobial properties of zinc oxide nanoparticles synthesized from *Lavandula pubescens* shoot methanol extract. *Applied Sciences* 2022; **12(22)**, 11613.

[29] S Shaheen, A Iqbal, M Ikram, M Imran, S Naz, A Ul-Hamid, A Shahzadi, W Nabgan, J Haider and A Haider. Graphene oxide-ZnO nanorods for efficient dye degradation, antibacterial and *in-silico* analysis. *Applied Nanoscience* 2022; **12**, 165-177.

[30] Mohammed, JK Oleiwi, AJM Jawad, AM Mohammed, AF Osman, R Rahman, T Adam, BO Betar, SCB Gopinath and OS Dahham. Effect of zinc oxide surface treatment concentration and nanofiller loading on the flexural properties of unsaturated polyester/kenaf nanocomposites. *Heliyon* 2023; **9(9)**, e20051.

[31] S Pethuan, N Tammachat, C Kaew-On, R Siri, N Tohluebaji, P Channuie and J Yuennan. Transparent P(VDF-HFP) coatings for enhancing fungal resistance, hydrophobicity, and durability of Krajood-based natural fibers. *Trends in Sciences* 2025; **22(7)**, 10441.

[32] R Șomoghi, A Semenescu, V Pasăre, OR Chivu, DF Nițoi, DF Marcu and B Florea. The impact of ZnO nanofillers on the mechanical and anti-corrosion performances of epoxy composites. *Polymers* 2024; **16(14)**, 2054.

[33] J Yuennan, S Nawae, N Tohluebaji, C Putson and N Muensit. Preparation of superhydrophobic surface on P(VDF-HFP) fibers by electrospinning technique. *Journal of Physics: Conference Series* 2021; **1719**, 012069.

[34] N Tohluebaji, R Siri, N Muensit, C Putson, P Channuie, P Porrawatkul and J Yuennan. Hydrophobic and optical properties of P(VDF-HFP) nanofiber filled with Nickel (II) chloride hexahydrate for dye-sensitized solar cells application. *Trends in Sciences* 2024; **21(9)**, 8762.

[35] Y Zhai and J Yang. Fabrication and modification of PVDF membrane by PDA@ZnO for enhancing hydrophilic and antifouling property. *Arabian Journal of Chemistry* 2023; **16**, 105206.

[36] C Du, Z Wang, G Liu, W Wang and D Yu. One-step electrospinning PVDF/PVP-TiO2 hydrophilic nanofiber membrane with strong oil-water separation and anti-fouling property. *Colloids and Surfaces A: Physicochemical and Engineering Aspects* 2021; **624**, 126790.

[37] BK Čech, H Sylva, Š Kateřina, R Michal and K Jana. Hybrid antibacterial nanocomposites based on the Vermiculite/Zinc oxide-chlorhexidine. *Journal of Nanoscience and Nanotechnology* 2019; **19(5)**, 3041-3048.

[38] Y Wang, D Lei, L Wu, N Hu, H Ning, Alamusi and Y Liu. Preparation of PVDF-HFP/CB/Ni nanocomposite films for piezoelectric energy harvesting. *Reviews on Advanced Materials Science* 2023; **62**, 20230146.

[39] S Paliwal, SK Gupta and CMS Negi. Structure–property correlation in PVDF-HFP/Carbon black nanocomposites: Insights from XRD, FESEM, and raman studies. *Journal of Macromolecular Science, Part B* 2026; **16**(34), 32496-32512.

[40] N Sedefoglu. Characterization and photocatalytic activity of ZnO nanoparticles by green synthesis method. *Optik* 2023; **288**, 171217.

[41] N Tohluebaji, N Muensit, C Putson, GA Ashraf, P Channuie, P Porrawatkul, U Wanthong and J Yuennan. Multi-functional enhancement of P(VDF-HFP) nanocomposites through MWCNTs loading for piezoelectric sensing. *Journal of Materials Research and Technology* 2025; **36**, 8475-8491.

[42] HH Singh, S Singh and N Khare. Enhanced β-phase in PVDF polymer nanocomposite and its application for nanogenerator. *Polymers for Advanced Technologies* 2017; **29(1)**, 143-150.

[43] P Kumar, M Mohil, S Negi, J Sharma, NNK Borah, Siddhartha, M Singh, C Kapoor, MI Quresh and MM Haque. Sustainable fabrication of ZnO nanorod/PVDF nanocomposites for ultraviolet photodetection and energy harvesting. *SPE Polymers* 2025; **6(3)**, e70014.

[44] SP Muduli, L Lipsa and S Parida. Current trends of characterization techniques for PVDF and related composite piezoelectric materials for nanogenerator. *Discover Polymers* 2025; **2**, 14.

[45] N Tohluebaji, C Putson, N Muensit and J Yuennan. Electrostrictive and structural properties of Poly(Vinylidene Fluoride-Hexafluoropropylene) composite nanofibers filled with Polyaniline (Emeraldine Base). *Polymers* 2021; **13(19)**, 3250.

[46] AU Khan, N Malik, B Singh, NH Ansari, M Rehman and A Yadav. Biosynthesis, and characterization of zinc oxide nanoparticles (ZnONPs) obtained from the extract of waste of

strawberry. *Journal of Umm Al-Qura University for Applied Sciences* 2023; **9**, 268-275.

[47] J Yuennan, C Nateethorn, P Samakphong, R Siri, N Tohluebaji, GA Ashraf, A Khanklaeo and P Channuie. Structural and shielding properties of P(VDF-HFP)-Bi2O3 multilayered polymer composites. *Journal of Science: Advanced Materials and Devices* 2025; **10(4)**, 100990.

[48] C Shee, S Banerjee, S Bairagi, A Baburaj, KSK Naveen, AK Aliyana, DM Mulvihill, R Alagirusamy and SW Ali. A critical review on polyvinylidene fluoride (PVDF)/Zinc oxide (ZnO)-based piezoelectric and triboelectric nanogenerators. *Journal of Physics: Energy* 2024; **6(3)**, 032001.

[49] M Spasova, N Manolova, N Markova and I Rashkov. Tuning the properties of PVDF or PVDF-HFP fibrous materials decorated with ZnO nanoparticles by applying electrospinning alone or in conjunction with electrospraying. *Fibers and Polymers* 2017; **18**, 649-657.

[50] OV Zakharova, IA Vasyukova, SP Chebotaryova, EY Koiava, SS Razlivalova, GV Grigoriev, PA Baranchikov and AA Gusev. Dose-dependent effects of ZnO nanoparticles towards the microalgae lobosphaera: Compensation of salt stress at low concentration and toxicity at high concentrations. *International Journal of Molecular Sciences* 2025; **26(19)**, 9455.

[51] H Ali, S Ali, K Ali, S Ullah, PM Ismail, M Humayun and C Zeng. Impact of the nanoparticle incorporation in enhancing mechanical properties of polymers. *Results in Engineering* 2025; **27**, 106151.

[52] A Sharma, K Akash, S Kumari, K Chauhan, A James, R Goel, J Singh, R Nagraik and D Kumar. Biogenic zinc oxide nanoparticles: An insight into the advancements in antimicrobial resistance. *ECS Journal of Solid State Science and Technology* 2024; **13(4)**, 047002.

[53] K Kalra, V Chhabra and N Prasad. Antibacterial activities of zinc oxide nanoparticles: A mini review. *Journal of Physics: Conference Series* 2022; **2267**, 012049.

[54] NM Elmayah, MI Abou-Dobara, ZAM Baka, A Elgaml, AE Khodir, HM Salama and MM El-Zahed. A novel green synthesized ZnO-based antimicrobial nanocomposite: Synergistic action, *in vitro* cytotoxicity, and molecular docking studies of ceftazidime, metformin, and chitosan against multidrug-resistant *Salmonella enterica*. *Microbial Cell Factories* 2026; **25**, 58.

[55] A Popova, DY Advakhova, AN Sheveyko, KA Kuptsov, P Slukin, SG Ignatov, A Ilnitskaya, RV Timoshenko, AS Erofeev, AA Kuchmizhak, B Subramanian and DV Shtansky. Synergistic bactericidal effect of Zn^{2+} ions and reactive oxygen species generated in response to either UV or X-ray irradiation of Zn-Doped plasma electrolytic oxidation TiO_2 coatings. *ACS Applied Bio Materials* 2024; **7(8)**, 5579-5596.

[56] P Porrawatkul, P Nuengmatcha, A Kuyyogsuy, R Pimsen and P Rattanaburi. Effect of Na and Al doping on ZnO nanoparticles for potential application in sunscreens. *Journal of Photochemistry and Photobiology B: Biology* 2023; **240**, 112668.

[57] L Zhang, M Yan, X Li, C Chen, J Ma and Z Wang. Interfacial interaction between Zn^{2+} and surface functional groups impacting self-assembly of ZnO on cellulose nanofibrils. *Langmuir* 2024; **40(44)**, 23415-23423.

[58] P Porrawatkul, R Pimsen, A Kuyyogsuy, P Rattanaburi and P Nuengmatcha. Morphology-dependent photocatalytic performance of ZnO nanostructures in organic dye and antibiotic degradation. *International Journal of Environmental Science and Technology* 2024; **21**, 7397-7414.